

Full length article

The grain-boundary structural unit model redux

Jian Han ^a, Vaclav Vitek ^a, David J. Srolovitz ^{a, b, *}^a Department of Materials Science and Engineering, University of Pennsylvania, Philadelphia, PA 19104, USA^b Department of Mechanical Engineering and Applied Mechanics, University of Pennsylvania, Philadelphia, PA 19104, USA

ARTICLE INFO

Article history:

Received 22 February 2017

Received in revised form

27 April 2017

Accepted 1 May 2017

Available online 3 May 2017

Keywords:

Grain boundaries

Structural unit model

Metastability

Simulation

ABSTRACT

Properties of grain boundaries (GBs) and their underlying structures are key to understanding polycrystalline material phenomena. The most widely used model for GB structure is the structural unit model (SUM), introduced ~ 50 years ago. The SUM represents GB structure as a combination of structural units (SUs); this combination evolves systematically with GB misorientation. Despite its successes, many observations suggest the SUM does not completely describe the GB structure; its utility for predicting GB properties is limited. There has been a growing realization that, even for fixed misorientation, multiple stable/metastable structures are common (corresponding to different microscopic degrees of freedom). We generalize the SUM by considering the effect of such metastable structures. While the SUM can describe GB structure evolution between a pair of delimiting boundaries, there will be many such evolutionary paths, corresponding to SUs associated with the metastable structure of the delimiting boundaries. The equilibrium GB energy vs. misorientation does not necessarily correspond to one of these paths, but will have contributions from many. Recognizing this, we propose a new approach to predict GB structure and energy, allowing for accurate determination of the GB energy vs. misorientation based on a very small number of atomistic simulations. For example, we predict the GB energy vs. misorientation for [100] and [111] symmetric tilt boundaries in BCC tungsten over the entire misorientation range to a mean error of <2 % based on atomistic simulations at only three or four misorientations. Our approach allows for the trade-off between computational cost and prediction accuracy.

Published by Elsevier Ltd on behalf of Acta Materialia Inc.

1. Introduction

The central goal of materials science is to establish the link between structure and properties. In a polycrystal, many properties may be traced to the properties/behavior of grain boundaries (GBs). Hence, the link between polycrystal properties, GB properties/behavior, and GB structure has been a recurring theme in materials science for nearly a century [1]. This paper focuses on a predictive model for GB structure and the link between the structure and GB properties, especially GB energy. Our approach is based upon some simple properties of single crystals, crystallography and minimal application of atomistic computer simulations (the number of such simulations is set by the desired overall accuracy of the prediction).

Starting from the early days of the study of GBs, there have been two distinct classes of GB structure models. The first class is the amorphous-cement model for high-angle GBs [2,3] which posits

that high-angle GBs are structureless. Although this model naturally leads to glass-like GB behaviors, intuitively consistent with the experimental measurement of viscous GB sliding [4], it contradicts direct observations in high-resolution microscopy [5,6] that routinely show highly ordered GB structures on the atomic scale. The second class of GB models is the dislocation model, such as those used to describe low-angle GBs [7–9]. Such models were extended to high-angle GBs by superimposing a dislocation structure onto a high-symmetry reference structure, rather than superimposing a set of isolated lattice dislocations on a single crystal [10–12]. In this model, we can think of the GB as consisting of a core, associated with the reference structure, and the elastic deformation associated with the elastic field of the dislocation array (this language is similar to that for a lattice dislocation, where we distinguish the long-range elastic field from a nonlinear core). The inherent weakness of such models for high-angle GB structure is associated with the need to identify an appropriate reference structure (the choice of which is not unique). Although some reference structures are better than others, the dislocation model cannot guide such choices. For example, for a high-angle GB with a

* Corresponding author. Department of Materials Science and Engineering, University of Pennsylvania, Philadelphia, PA 19104, USA.

E-mail address: srol@seas.upenn.edu (D.J. Srolovitz).

misorientation angle close to that of a coherent twin boundary, we can choose either a single crystal or the coherent twin boundary as the reference structure. Observation of the atomic structure of this GB shows that this boundary is almost identical to that of the coherent twin boundary except for the addition of widely separated dislocations. Clearly, in this case, the coherent twin boundary provides a much better reference than does the single crystal. Identification of a good reference structure can only be made by considering the atomic structure of a GB. For low-angle GBs, the obvious reference structure is the single crystal and hence the dislocation model can be directly applied; however, the predictability of the dislocation model for high-angle GBs is limited (without knowledge of the atomic structure of the GB core).

The inherent weakness of the dislocation model for high-angle GBs is mitigated by the structural unit model (SUM) [13–16], which explicitly accounts for the atomic structure of the GB core. The SUM supplements the dislocation model through knowledge of the atomic structure of several specific GBs, which often possess high symmetry, as determined through atomistic simulations or experiments. These specific GBs, called “delimiting boundaries”, serve as the reference structures for all other GBs. The structure of a GB that is geometrically between two delimiting boundaries can be described as a combination of the SU associated with these two delimiting boundaries; the minority units simply corresponds to the (secondary) dislocations in the dislocation model for high-angle GBs.

Despite the successes of the SUM, experimental and atomistic simulation results accumulated over the half-century since its introduction show that there is a large (and growing) set of cases for which the SUM simply does not work. For example, even for pure tilt GBs with low-index rotation axes, the structures of the intervening boundaries cannot be predicted based on the structures of the delimiting boundaries [17,18]. Perhaps these discrepancies between the SUM and the experimental/simulation observation is the result of not choosing the correct reference structures. By initially examining more conceivable reference structures, it may be possible to provide the correct prediction. Another possible source of the discrepancy is associated with the fact that for many boundaries a single, unique structure does not exist; i.e., there are multiple, metastable structures [19–24]. Unfortunately, identifying more potential delimiting boundaries or determining more structures for each GB would require additional (and often expensive/time consuming) simulations or measurements. Hence, this implies an inherent trade-off between accuracy and efficiency. Finally, we note that GB structure can change with temperature or in the course of some dynamical processes (e.g., absorption of point defects during irradiation, absorption of dislocations during plastic deformation, or GB sliding). In fact, examination of GB kinetic effects (such as GB sliding) seems to support the amorphous-cement model [25–27] rather than the SUM, which is inherently based upon crystallography. Despite these challenges, the SUM remains the most widely used approach for describing/predicting GB structure (e.g. Ref. [28]) and GB properties (e.g. Refs. [29–31]).

Grain-boundary metastability or multiplicity is a unifying feature associated with the issues raised above. GB metastability refers to the existence of different microscopic or atomic structures for a fixed set of macroscopic GB descriptors (i.e., rotation axis, misorientation angle and GB plane normal). We note that at high temperature or during dynamical processes, the GB does not necessarily occupy only its ground state (structure with the minimum energy) but may explore many metastable states [24]. Inclusion of GB metastability in the SUM is key to understanding the observed GB structure/properties and how these evolve with the GB geometry, as well as glass-like GB behavior which is normally

thought of as a feature of the amorphous-cement model and a failure of the SUM.

In this paper, our goals in revisiting the SUM are two-fold: (1) to generalize the SUM to address why it leads to frequent erroneous predictions of GB structure/energy and (2) to develop an approach to predict GB structure and energy as a function of crystallographic variables with an accuracy that can be iteratively improved with increasing number of atomistic simulations. In the next section, we discuss GB geometry and the method we employ in atomistic simulations of GB structure. Then, we describe the atomic structure of the GBs in terms of a generalized SUM. In the following section, we develop a practical, efficient approach for predicting the GB energy (and other properties) in terms of the generalized SUM and a small set of atomistic simulations.

2. Macroscopic geometry and atomistic simulation method

For the sake of simplicity and clarity, we focus our discussion on the case of symmetric tilt grain boundaries (STGBs) in cubic metals. In addition, we further focus on those STGBs which have a periodic atomic structure (i.e., coincidence-site-lattice (CSL) GBs). This is a relatively weak assumption since any non-periodic (irrational) GB can be approximated as a periodic boundary to any degree of accuracy required.

We create any such STGB in a cubic crystal as follows. First, construct a cubic crystal, choose a mirror plane, and establish a Cartesian coordinate system $\hat{\mathbf{o}} \times \hat{\mathbf{p}} \times \hat{\mathbf{n}}$, where $\hat{\mathbf{o}}$ and $\hat{\mathbf{p}}$ are parallel and $\hat{\mathbf{n}}$ is perpendicular to the mirror plane. We define $\hat{\mathbf{o}}$ to be the tilt axis. Rotate the crystal by $\theta/2$ about the $\hat{\mathbf{o}}$ -axis (i.e., the tilt axis). Repeat this procedure for another (identical) crystal but rotate it by $-\theta/2$ about the $\hat{\mathbf{o}}$ -axis. Remove all of the atoms from the first crystal below the mirror plane and those from the other crystal above the mirror plane. Join the two half-crystals to create the GB. This mirror plane is the GB plane and the GB has a misorientation angle of θ about the $\hat{\mathbf{o}}$ -axis.

When the crystallographic indices of the $\hat{\mathbf{o}}$ - and $\hat{\mathbf{p}}$ -directions are rational, there are an infinite number of discrete values of the misorientation angle θ such that the two lattices coincide at a subset of the lattice sites. The GB formed in this way is called a CSL GB. The reciprocal of the fraction of sites which are coincident is denoted Σ . A CSL GB is periodic in both the $\hat{\mathbf{o}}$ - and $\hat{\mathbf{p}}$ -directions. Denote the period vector along the $\hat{\mathbf{o}}(\hat{\mathbf{p}})$ -axis by \mathbf{o} (\mathbf{p}), with magnitude o (p) equal to the boundary period.

While the SUM approach we describe in this paper is applicable to all crystalline materials, for concreteness, we choose our examples to be GBs in a body-centered cubic (BCC) metal; in atomistic studies a many-body Finnis-Sinclair interatomic potential developed for tungsten [32] has been used. Although this potential is indeed able to produce many properties of tungsten, it is considered here as a representative model of a BCC metal. The first step in our atomistic simulations is to construct bicrystal supercells for [100] and [111] tilt axes and several misorientations, as listed in Table 1. In order to explore possible metastable GB structures, we construct supercells for each misorientation in which we displace the upper crystal relative to the lower crystal by a displacement vector that lies within the GB plane. We explore a sufficient number of possible shifts to ensure that we capture nearly all possible metastable GB structures, as described in detail in Ref. [24]. Starting from each of these initial structures (we explore the cases for two tilt axes, 162 misorientations, and many shifts corresponding to a total of 130,000 structures), we relax the structures via a conjugate-gradient energy minimization procedure. These simulations represent the data set against which we compare our predictions.

We emphasize that different atomistic simulation methods may

Table 1

Bicrystal geometry for the [100] and [111] STGBs: \mathbf{o} is the tilt axis, \mathbf{n} is the GB plane normal, and \mathbf{p} is a vector along the direction $\mathbf{n} \times \mathbf{o}$. Also listed are the number of the GBs constructed with different misorientations (N_{GB}), the entire misorientation range ($\Delta\theta$) and the maximum Σ value considered in this study (Σ_{max}). Note, the indices k and l are integers and satisfy $0 < k \leq l$.

\mathbf{o}	\mathbf{p}	\mathbf{n}	N_{GB}	$\Delta\theta (\circ)$	Σ_{max}
[100]	$[0, k, l]/[0, \bar{k}, \bar{l}]$	$[0, \bar{l}, k]/[0, \bar{l}, \bar{k}]$	110	$[0, 90]$	941
[111]	$[k, l, \bar{k} + \bar{l}]/[l, k, \bar{k} + \bar{l}]$	$[\bar{k} + 2l, 2k + l, l - k]/[2\bar{k} + l, k + 2l, \bar{l} - \bar{k}]$	52	$[0, 60]$	1569

find different GB structures. For example, a genetic algorithm or simulated annealing approach will more likely find the minimum-energy GB structures than the conjugate-gradient minimization approach on a (relatively) small unit employed here. Nonetheless, the goal here is to find all of the stable and metastable GB structures. Hence, methods such as genetic algorithms or simulated annealing are not appropriate here.

3. Grain-boundary structure

3.1. Original structural unit model

Before beginning our analysis of GB structure, we briefly summarize several important ideas from the original SUM.

- (1) *Structural Unit Representation* [13,14]. A GB structure can be described as a combination of building blocks or structural units (SUs) in two dimensions. For example, the structures of the [100] STGBs corresponding to misorientations $\theta = 0$ and 36.87° are composed of only “A” unit and only “C” unit, respectively (see Fig. 1). Note that the “A” unit simply describes the (001) plane of the BCC crystal. On the other hand, the structure of the $\theta = 22.62^\circ$ STGB is composed of both “A” and “C” units in a 1 : 1 ratio; we describe this structure as |AC·AC|, where the vertical lines denote one GB period along the $\hat{\mathbf{p}}$ -axis and “·” indicates that the two neighboring SUs are shifted along the $\hat{\mathbf{o}}$ -axis by a half period with respect to each other. Following the same notation, the structure of the $\theta = 18.92^\circ$ STGB is |AC·AAC|, where the ratio of “A” to “C” units is 3 : 2. In the SUM, the atomic structure of an entire GB is represented by combination of individual SUs, each with a well defined atomic structure (GB core structure), rather than as an array of dislocations.
- (2) *Structural Unit Combination* [14,15]. Grain boundaries that are composed of a single type of SU are termed delimiting [33]. The structure of any boundary with θ in the misorientation range bounded by two neighboring delimiting boundaries

(called intervening boundary) is composed of the SUs of these two delimiting boundaries. The ratio of the numbers of the two types of SUs in a boundary varies monotonically with θ . For example, as shown in Fig. 1, the boundaries at $\theta = \theta_A = 0$ and $\theta = \theta_C = 36.87^\circ$ are delimiting. The structure of any boundary with $0 < \theta < 36.87^\circ$ is composed of n_A “A” units and n_C “C” units in the ratio

$$\frac{n_A}{n_C} = \frac{p_C}{p_A} \frac{\sin[(\theta_C - \theta)/2]}{\sin[(\theta - \theta_A)/2]}, \quad (1)$$

where p_A and p_C are the sizes of the unstrained “A” and “C” units (see Fig. 1), respectively, along the $\hat{\mathbf{p}}$ -axis. This rule enables the SUM to predict the θ -dependence of the GB structure. The definition of a SU is not fixed, however. For example, we could denote the entire structure associated with one period of the $\theta = 22.62^\circ$ GB as a single structural unit (replacing “AC”), in which case it would be considered delimiting. Such SUs that can be decomposed into other SUs are termed multiple unit reference structures (MURS) in the literature [34]. The structure of any GB with $0 < \theta < 22.62^\circ$ can be described as composed of A and [AC] units, where $[.]$ denotes MURS (see the structure of the $\theta = 18.92^\circ$ GB in Fig. 1, which is |AC·A[AC]|).

(3) *Structural Unit Sequence* [16]. The sequence of SUs in a GB may be deduced from a simple energy argument. If we describe the minority SU in a GB as a (secondary) GB dislocation (the elastic field around such a minority SU is consistent with it being a dislocation), the lowest energy arrangement of SUs will be that in which the spacing between these SUs is as uniform as possible. For example, the structure of the $\theta = 18.92^\circ$ GB is |AC·AAC| rather than |AAAC·C| (see Fig. 1), because “C” units are more uniformly separated in the former sequence rather than aggregated as in the latter sequence.

The first of these SUM ideas is true, in the sense that we can successfully describe the structure of any (periodic or CSL) GB as a series of SUs. While there may be many ways to draw a SU, any such unit that has the correct period is equally valid. The second of these SUM ideas is, however, problematic. There are many observations

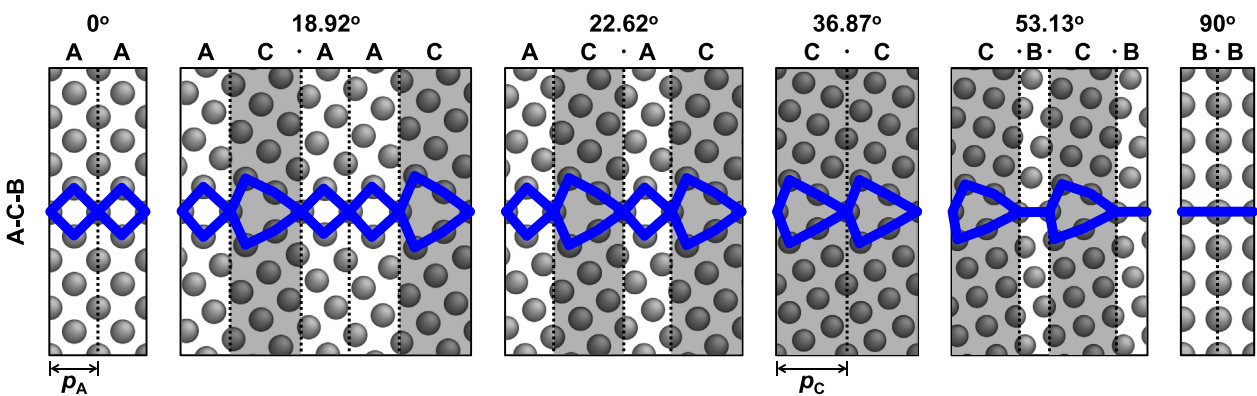


Fig. 1. GB structures represented by “A”, “B” and “C” units. Each SU is delineated by the dotted lines and outlined by the blue solid lines. The misorientation θ and the SU representation are indicated above each figure. (For interpretation of the references to colour in this figure legend, the reader is referred to the web version of this article.)

from atomistic simulations which show that the GB structure corresponding to a θ value between two delimiting boundaries is not composed of the SUs of those delimiting boundaries [17,18]. This is also the case for many GBs simulated in this paper, as discussed below. The third of these SUM ideas is consistent with obtaining the minimum-energy GB structure for each θ . However, this idea can be violated in nonequilibrium situations, in which case higher-energy SU sequences may be observed [1].

3.2. Metastable structural unit model

As discussed above, there is ample evidence suggesting that a GB with fixed macroscopic degrees of freedom may have one of several different atomic structures, one of which is thermodynamically stable (with the minimum free energy) and the others are metastable (i.e., stable against perturbation but with higher energy than the stable structure). We refer to these collectively as metastable structures. The original SUM focuses on the single stable structure for each of the delimiting boundaries. We now generalize the SUM to account for the possibility of several different metastable SUs for the delimiting boundary. In particular, we examine how these metastable structures influence the overall GB structure (and energy) as a function of the misorientation θ . We demonstrate that accounting for the metastability in the delimiting boundaries alleviates the issue with the original SUM labeled (2) above, i.e., the existence of GB structures with SUs inconsistent with the delimiting boundaries.

In Fig. 2 (a), we show the GB energy $\gamma(\theta)$ as a function of misorientation θ (symmetric tilt GBs with a [100] tilt axis) in tungsten, as we reported earlier [24]. The main conclusion to be drawn from this figure is that (nearly) every GB has multiple, metastable structures (indicated by the grey data points) and that the number of such metastable structures corresponding to each misorientation can be very large. For the misorientations we examined in tungsten, we find as many as 273 metastable structures for a particular θ (this is at $\theta = 51.3^\circ$). Close examination of the GB structures in this plot shows that there is not a single structure-evolution path along the θ -axis (as in the original SUM), but rather many such paths. We demonstrate this explicitly below. Based on this observation, we present a generalized or metastable structural unit model (MSUM).

3.2.1. $0 \leq \theta \leq 90^\circ$ boundaries

First, we examine the SUs corresponding to two special

misorientations $\theta = 0$ and 90° . These misorientations are in fact not misorientations at all but rather represent the (001) and (011) planes of the perfect BCC crystal. We label the corresponding SUs as "A" and "B", respectively (see Fig. 3(a)). According to the original SUM, we might expect that the structure of any [100] STGB is a combination of "A" and "B" units. However, as foreseen in the SUM, this does not work well since large misorientation deviation from these delimiting GBs necessarily implies that "A" and "B" units will be greatly distorted. For example, consider the case of the $\theta = 36.87^\circ$ GB which, according to Eq. (1), can be described as alternating "A" and "B" units, i.e., $|AB \cdot AB|$. Comparing the periods of the $36.87^\circ |AB \cdot AB|$ structure with those of the "A" and "B" units demonstrates that on average these SUs are compressed by 7.4%. While the $|AB \cdot AB|$ structure of the $\theta = 36.87^\circ$ GB (see Fig. 3(a)) is metastable, its energy is very high. Atomistic simulations show that, for several misorientations in the $0 \leq \theta \leq 90^\circ$ range, the GB structure can indeed be described by combinations of "A" and "B" units. However, there are few such misorientations (indicated by the dark green crosses in Fig. 2(a)) and, where they do occur, the GB energy is very large (i.e., they are metastable). For all the other misorientations examined, there is no metastable structure which is purely a combination of "A" and "B" units.

Since the combination of "A" and "B" units leads to unstable or a high-energy metastable structure for the high-angle GBs, it is expected that the high-angle GBs may relax to a lower-energy configuration through reconstructions. While the structure $|AB \cdot AB|$ of the $\theta = 36.87^\circ$ GB is under severe compression (with high energy), a lower-energy structure can be obtained by lowering the atomic fraction in the GB region (i.e., through the reconstruction of the "AB" unit into a "C" unit) as shown in Fig. 1. The simulation result indeed shows that the stable structure of this GB is $|C \cdot C|$. Then, the structure of any GB with $0 < \theta < 36.87^\circ$ is composed of "A" and "C" units, while the structure of any GB with $36.87^\circ < \theta < 90^\circ$ is composed of "C" and "B" units (see Fig. 1). We find that the structure-evolution path characterized by the combination of "A", "C" and "B" units ("A-C-B path" for short) exists throughout the entire θ range (see the blue curve in Fig. 2(a)).

Although the existence of "C" units generally lowers the GB energy, the structures along the A-C-B path are not necessarily the minimum-energy structures; the deviation from the minimum-energy structures is enhanced in the $61.93^\circ < \theta < 90^\circ$ range (see Fig. 2(a)). We find that a "C" unit can be re-interpreted as two "E" units, i.e., " $C \equiv E \circ E$ " (see Fig. 3(b)), where " \circ " indicates that the two neighboring SUs are shifted along the \hat{n} -axis with respect to

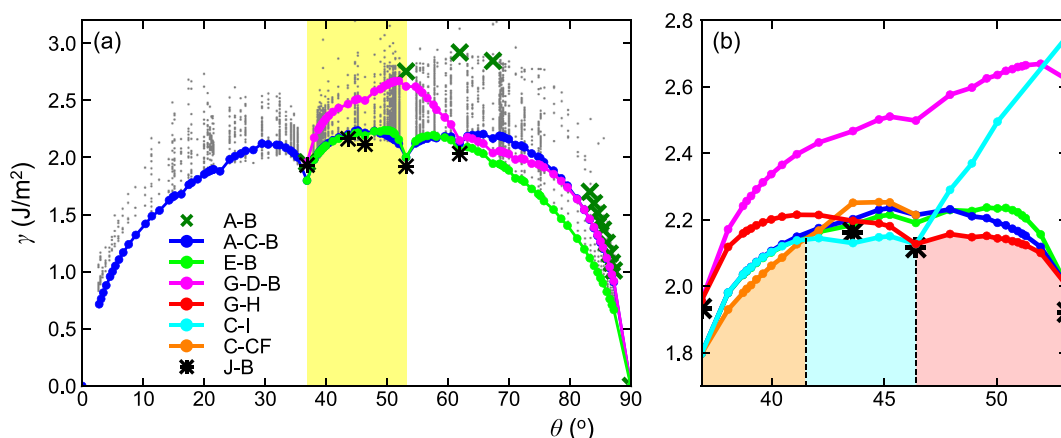


Fig. 2. (a) GB-energy (γ) spectrum of all metastable GB states (gray dots) for each misorientation (θ) associated with [100] STGBs in BCC tungsten, obtained from atomistic simulations. Several structure-evolution paths corresponding to the combination of different SUs are plotted. (b) An enlargement of the GB-energy spectrum for $36.87^\circ \leq \theta \leq 51.3^\circ$ (i.e., the yellow region in (a)). (For interpretation of the references to colour in this figure legend, the reader is referred to the web version of this article.)

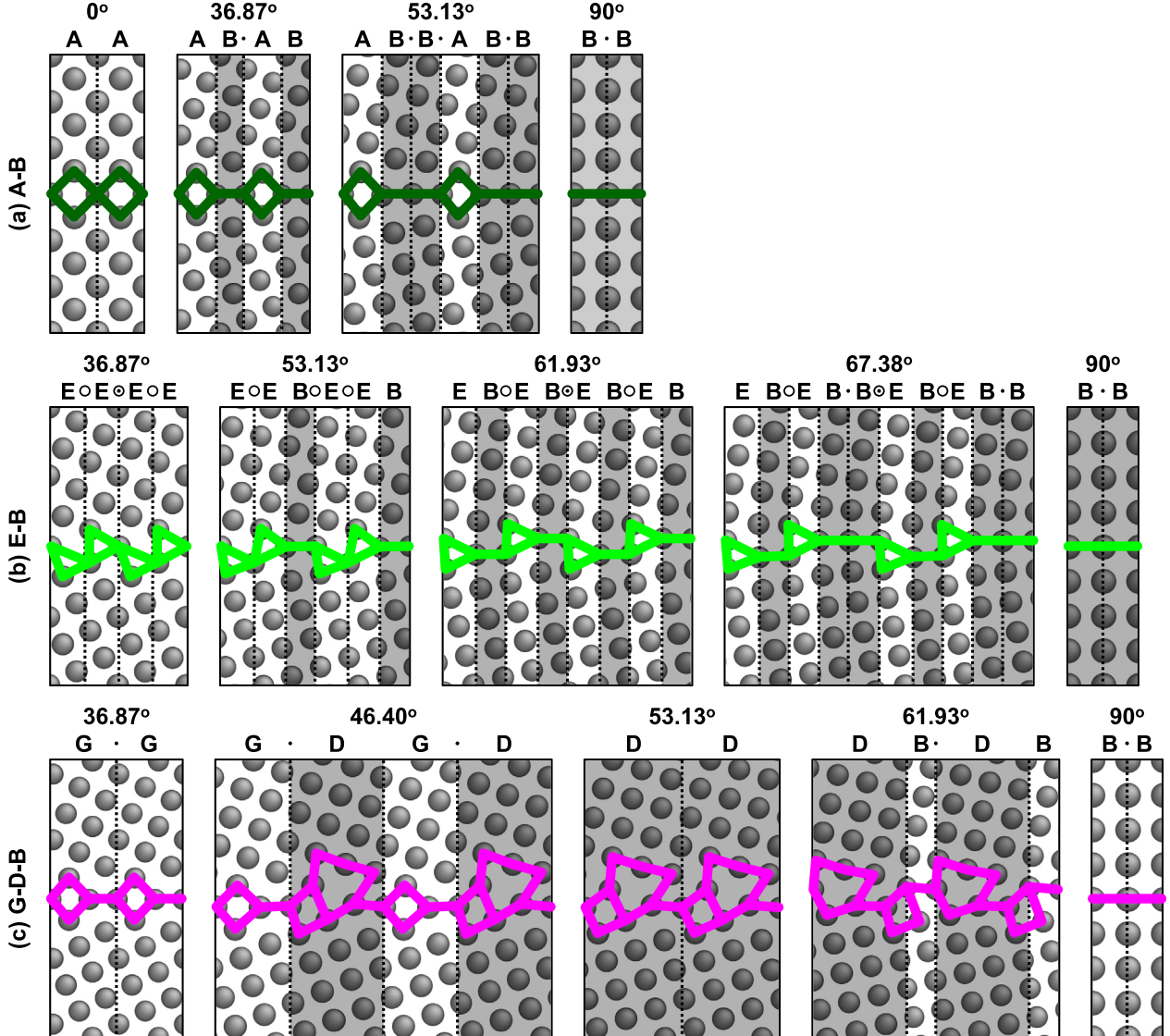


Fig. 3. GB structures represented by (a) “A” and “B” units, (b) “E” and “B” units, and (c) “G”, “D” and “B” units (“G” \equiv “AB”). The meanings of the symbols “ \cdot ”, “ \circ ” and “ \odot ” are described in the text.

each other. The combination of “E” and “B” units constitutes the most stable structures for low-angle GBs with θ near 90° (see Fig. 2(a)). This can be understood as follows. In this low-angle regime, any SU other than “B” units can be viewed as (secondary) GB dislocations [14], the elastic energy of which is determined by its Burgers vector and the dislocation spacing. Because the size of an “E” unit is half that of a “C” unit, in a low-angle GB, “E” represents a GB dislocation with Burgers vector and dislocation spacing half of those when it is represented by a “C” unit. Hence, the elastic energy of an array of “E” GB dislocations is smaller than that of an array of “C” GB dislocations (*cf.* the blue and the green curves in Fig. 2(a)).

Another example of an SU reconstruction is the $\theta = 53.13^\circ$ GB, where replacing the $|AB \cdot B|$ structure (Fig. 3(a)) with a “D” unit (Fig. 3(c)) lowers the energy. A series of metastable GB structures in the $36.87^\circ < \theta < 90^\circ$ range can be regarded as the combination of “G”, “D” and “B” units, where “G” is simply a shorthand for “AB”.

From the analysis above, we see that the SUM works well for each pair of stable/metastable SUs. The application of the SUM to all stable/metastable SUs results in multiple structure-evolution paths along the θ -axis (Fig. 2). However, it does not guarantee that the

minimum-energy GB structures (as function of θ) should follow the SUM, since some minimum-energy structures may belong to a particular structure-evolution path (e.g. A-C-B path) and others may belong to one of the other possible paths (e.g. E-B path). In other words, the minimum-energy path may be a combination of several different structure-evolution paths – this is one of our central observations. The reason path crossings occur may be understood as arising from the contributions of GB core energy and elastic energy. Here, the A-C-B path is associated with lower core energy (important for high-angle GBs), while the E-B path is associated with lower elastic energy (important for low-angle GBs).

3.2.2. $36.87^\circ \leq \theta \leq 53.13^\circ$ boundaries

Consideration of both the A-C-B and E-B paths provide a very good prediction of the minimum-energy GB structures over the entire range of misorientation θ . However, as we discuss in this section, these paths only predict the exactly correct minimum-energy GB structures for the low-angle GBs (i.e., near $\theta = 0$ and 90°). In particular, we focus here on the intermediate misorientation range $36.87^\circ < \theta < 53.13^\circ$, where we will see that the

minimum-energy structures do not lie on either the A-C-B path or the E-B path (see Fig. 2(b)). This suggests that other paths (corresponding to combinations of other SUs) represent the minimum energy structures for high-angle GBs.

As discussed above, there are multiple metastable structures for the two $\Sigma 5$ GBs at $\theta = 36.87^\circ$ (two structures) and $\theta = 53.13^\circ$ (three structures). For the $\Sigma 5 \theta = 36.87^\circ$ GB, the two metastable structures can be described as $|C \cdot C|$ (or, equivalently, $|E \odot E \odot E|$) and $|AB \cdot AB|$ (“ \odot ” indicates that the two neighboring SUs are shifted along the $\hat{\mathbf{o}}$ -axis by a half period and, at the same time, shifted along the $\hat{\mathbf{n}}$ -axis with respect to each other). For the $\Sigma 5 \theta = 53.13^\circ$ GB, the three metastable structures can be described as $|C \cdot B|$ (or, equivalently, $|E \odot EB|$), $|D|$ and $|AB \cdot B|$. We can select these two $\Sigma 5$ GBs as delimiting boundaries and define each of their metastable structures as SUs (i.e., MURS). Then, according to the SUM, we will have possible structure-evolution paths characterized by all possible pairings of MURS from each of the two delimiting $\Sigma 5$ GBs.

Since we consider the two $\Sigma 5$ GBs as delimiting boundaries, all intervening GBs are combinations of the SUs for these boundaries. Hence, instead of talking about the structure of the $\theta = 36.87^\circ$ GB as $|AB \cdot AB|$, we describe it as $|G \cdot G|$ or “G” \equiv “AB”. Similarly, we can write “H” \equiv “CB” for one of the structures for the $\theta = 53.13^\circ$ GB. Fig. 4(a) shows the structure-evolution path corresponding to the combination of “G” and “H” units (“G-H path”). The minimum energy in the $46.40^\circ < \theta < 53.13^\circ$ range (a part of the misorientation range between the two $\Sigma 5$ GBs) corresponds to the G-H path (red curve in Fig. 2(b)).

We now consider another structure of the $\Sigma 5 \theta = 36.87^\circ$ GB,

described as the “C” unit, and another structure of the $\Sigma 5 \theta = 53.13^\circ$ GB, described as the “I” unit (“I” \equiv “BAB”). Combinations of these (see the structures in Fig. 4(b)) constitute the C-I path (light blue curve in Fig. 2(b)). In Fig. 2(b), we see that, in the $41.50^\circ < \theta < 46.40^\circ$ range, the C-I path is, in fact, the minimum-energy path.

The minimum-energy structures in the $36.87^\circ < \theta < 41.50^\circ$ range cannot be obtained by combinations of the SUs which have already been defined. The minimum-energy structures are combinations of “C” and “F” units (“C-CF path”) as shown in Fig. 4(c), where “F” is another SU that is equivalent to a GB step. We note that there is no delimiting boundary composed only of “F” units – such a structure is unstable. This can be understood by analogy with buckling. As discussed above, the geometric constraints associated with fixing the misorientation of the GB implies that the GB is under compression (except for the delimiting GBs). This compression can lead to buckling of the GB, which is localized as creases or steps – this is the origin of the “F” GB steps (this type of localization of buckling gives rise to creases in other contexts [35]).

Examination of the GBs in the $36.87^\circ \leq \theta \leq 53.13^\circ$ range demonstrates that the minimum-energy path is, in fact, composed of three distinct paths which cross each other. The three paths correspond to C-CF, C-I, and G-H paths (see Fig. 2(b)). Along each of these paths, the SUM successfully describes the GB structure.

3.2.3. Summary of the metastable structural unit model

We can summarize the main results/concepts of the metastable structural unit model (MSUM) as follows:

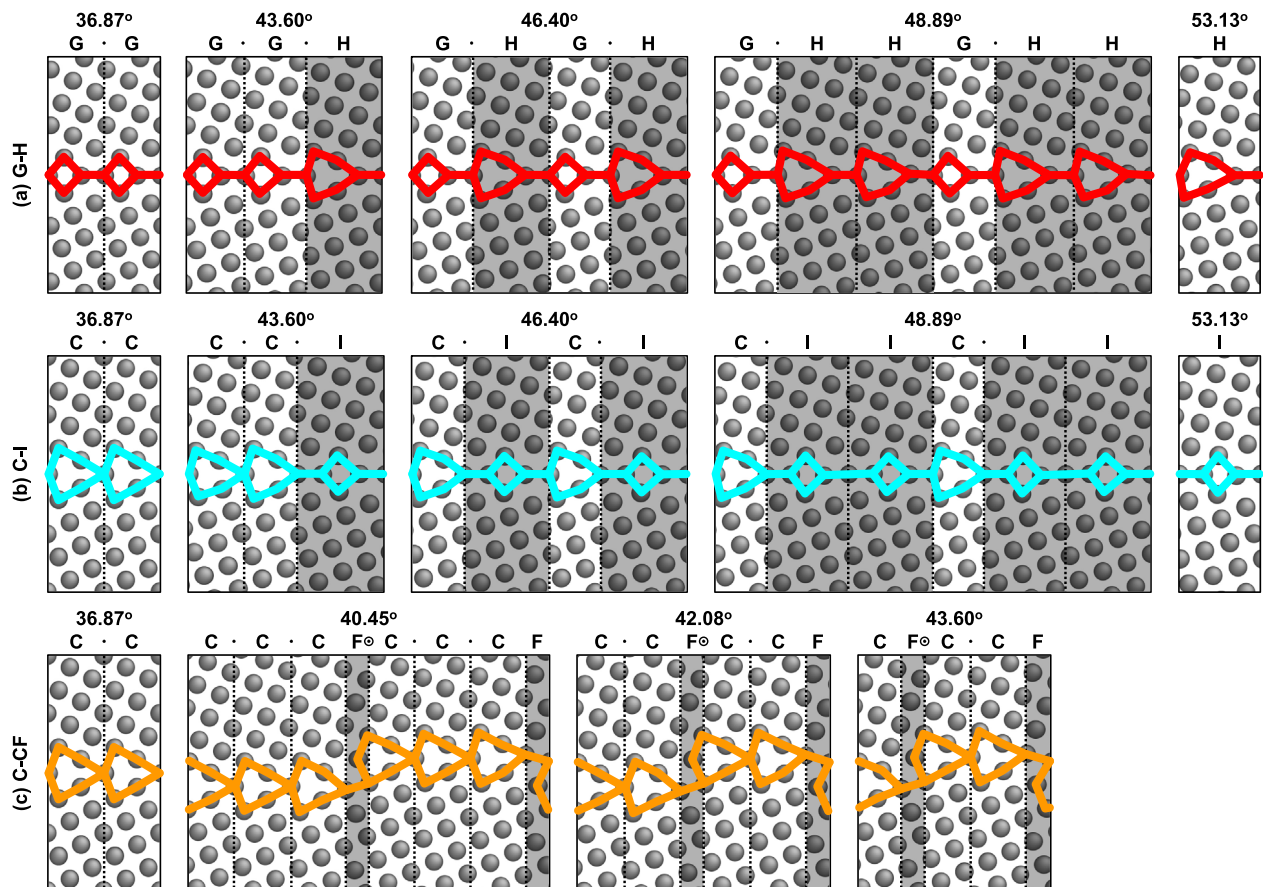


Fig. 4. GB structures represented by (a) “G” and “H” units, (b) “C” and “I” units, and (c) “C” and “CF” units (“G” \equiv “AB”, “H” \equiv “CB”, “I” \equiv “ABA”, and “F” unit represents a step on the GB).

- (1) Any GB structure can be represented as an ensemble of SUs. For any particular misorientation, there may be several different GB structures, depending on which of the stable or metastable SUs are present.
- (2) Any GB (with misorientation θ) can be described as an ensemble of the SUs of the two delimiting boundaries (θ lies between the misorientations of the two delimiting boundaries). Since the delimiting boundaries may have multiple metastable structures (with distinct SUs), there are multiple structures corresponding to all possible pairs of SUs from the two delimiting GBs. (Note, however, that some of these may be unstable and, hence, not observable.)
- (3) The best possible selection of the delimiting boundaries is not always obvious; however, such delimiting boundaries can be identified as follows. First, start from the two misorientations where the GB structures have the smallest period (usually associated with small Σ value). Second, identify the GB between these two misorientations which has the smallest period; this is another delimiting boundary. This step can be repeated *ad infinitum*; however, this procedure may be terminated at any point based, for example, on the accuracy to which the minimum-energy GB structure is required. Note that in the original SUM, the delimiting boundaries were chosen *a priori* based on the general idea that the misorientation range between delimiting boundaries was not too large. In the MSUM, there is a well-defined framework for identifying delimiting boundaries and iteratively improving this identification.
- (4) Application of the SUM to all the metastable GB structures leads to multiple structure-evolution paths along the θ -axis (see Fig. 2). The number of metastable paths grows rapidly with the number of iterations of delimiting boundary selection (i.e., step two in (3)).

We now exploit the MSUM to predict GB energy and its variation with misorientation.

4. Grain-boundary energy

The grain-boundary energy is the central thermodynamic descriptor of a GB and, hence, it figures prominently in analyses of many phenomena such as grain growth, GB wetting, heterogeneous nucleation of new phases, and solute segregation in polycrystals [36]. Not surprisingly, this has led to intense efforts to predict GB energy from macroscopic GB descriptors, such as macroscopic GB geometry. Since a fundamental tenet of materials science is that properties are related to structure, such efforts have largely focused on connecting GB geometry to GB structure to GB energy. For example, the classical Read-Shockley equation for the energy of low-angle GBs [9] is based on a description of the spacing between the dislocations that compose the GB structure and that spacing to the GB misorientation [7]. More recently, an expression for high-angle GB energy based on a generalization of the Read-Schrockley approach in terms of Frank's formula for GB dislocation content [37] was introduced. Another representation of the GB energy for the entire five-dimensional GB macroscopic geometry space was proposed [38]. The resultant dislocation model-based energy description qualitatively captures several trends in the variation of the GB energy with misorientation, but cannot predict the ubiquitous cusp features of the GB energy vs. misorientation (e.g. see Fig. 5.23 in Ref. [1]) and relies on fits to large quantities of experimental and/or atomistic simulation data. We believe that this is because these dislocation models do not appropriately treat the GB core energy (i.e., the energies of the delimiting boundaries). Another approach to predict GB energy is based on the “lattice

matching” of the surfaces of the two grains that meet at the GB [39]. This approach, at least in spirit, accounts for the GB core effect; e.g., it can predict the location of the cusps on the GB energy vs. misorientation without fitting. However, this model does not lead to reliable GB energy predictions (e.g., the depth of the energy cusps). We believe that this is because this approach does not account for the elastic energy associated with the dislocation structure of the GBs (which is applicable even at large misorientations).

Wang and Vitek [40] proposed an approach to predict GB energy based on the SUM that includes both the elastic and GB core energies [40]. This model had only marginal success, because of the inherent limitations of the original SUM. For example, the results and discussion above demonstrate that the (minimum) GB energy vs. misorientation depends not on one structure-evolution path (as in the original SUM) but on many paths (as in the MSUM). We now present a strategy for predicting the GB energy vs. misorientation that includes both the contributions of elasticity and the GB core based upon limited GB energy data (e.g., from simulation) which can be iteratively improved to achieve desired accuracy with minimal input.

4.1. Analytical preliminaries

In this section, we address the question of the prediction of GB energy vs. misorientation given basic properties of the delimiting boundaries. Identification of the delimiting boundaries is deferred to later. For the two delimiting boundaries (one composed of “X” units and the other “Y” units), we know the misorientations θ_X and θ_Y ($\theta_Y > \theta_X$), the periods p_X and p_Y , and the energies γ_X and γ_Y . To predict the energy of the intervening boundaries, we partition the GB energy as $\gamma = \gamma^c + \gamma^{el}$, where γ^c is the GB core energy attributed to the energies of the two delimiting boundaries, and γ^{el} is the elastic energy within the grains.

4.1.1. GB core energy

From Eq. (1), we know the numbers of “X” and “Y” units per GB period, n_X and n_Y . The simplest approximation for the GB core energy is as a weighted average of the energies of these SUs:

$$\gamma^c(\theta) = \frac{1}{p} \left[n_X p_X \cos\left(\frac{\theta - \theta_X}{2}\right) \gamma_X + n_Y p_Y \cos\left(\frac{\theta_Y - \theta}{2}\right) \gamma_Y \right], \quad (2)$$

where the GB period p is

$$p = n_X p_X \cos\left(\frac{\theta - \theta_X}{2}\right) + n_Y p_Y \cos\left(\frac{\theta_Y - \theta}{2}\right). \quad (3)$$

For example, we evaluate the core energies of the $36.87^\circ \leq \theta \leq 53.13^\circ$ GBs along the G-H path (see Fig. 4(a)) via Eq. (2) by setting “X” = “G” and “Y” = “H”; the result is shown as the blue solid curve in Fig. 5(a).

In Eq. (2), we ignored the interactions between “X” and “Y” units; this leads to errors which are especially important around the middle of the misorientation range ($\theta = 46.40^\circ$). We can improve this estimate if we know the core energy of one or more intervening boundaries. For example, we can estimate the interaction energy between the “X” and “Y” units from the energy of the GB composed of alternating “XY” units, where we denote the energy and misorientation by γ_{XY}^c and θ_{XY} . For $\theta_X < \theta < \theta_{XY}$, we can apply Eq. (2) by replacing Y with XY and γ_Y with γ_{XY}^c and, for $\theta_{XY} < \theta < \theta_Y$, we replace X with XY and γ_X with γ_{XY}^c . In practice, we can obtain γ_{XY}^c by $\gamma - \gamma^{el}$ for the GB with $\theta = \theta_{XY}$, where γ is from the simulation data and γ^{el} is estimated by the formula given in the next section. Returning to the example of G-H path, we see that introducing the “GH” unit changes the core energy of the G-H path

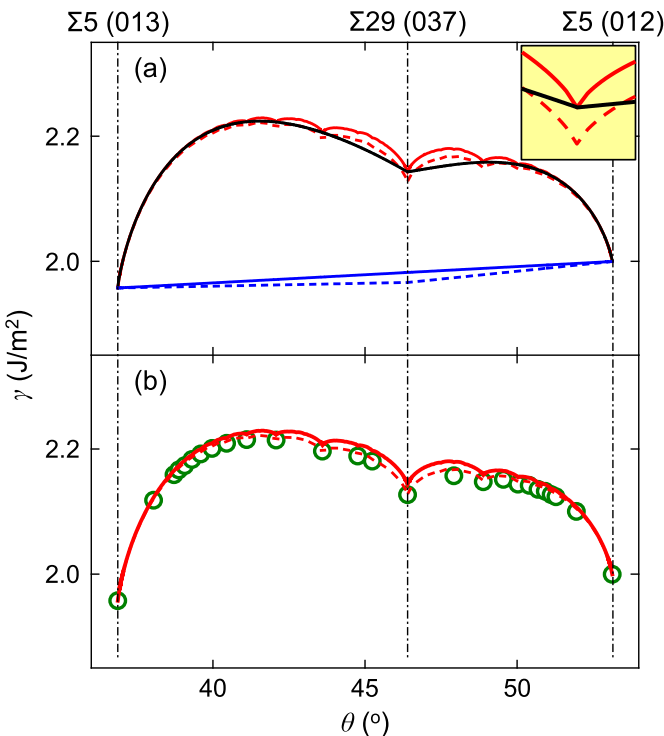


Fig. 5. (a) shows the GB core energy γ^c (blue solid curve), the total GB energy γ without recursion (black solid curve) and γ with five recursion steps (red solid curve) predicted for the G-H path (ref. Fig. 4(a)) based on the knowledge of the structures and energies of two $\Sigma 5$ GBs. The inset shows the detail about $\theta = 46.40^\circ$. (b) shows the comparison between the predicted γ (red solid curve) and the simulation data (dark green circles). The blue and the red dashed curves correspond to the GB core energy and the total GB energy, respectively, predicted with an extra (simulation) data point (at $\Sigma 29$ (037)) used in the prediction. (For interpretation of the references to colour in this figure legend, the reader is referred to the web version of this article.)

from the blue solid curve to the dashed one in Fig. 5(a). The fact that the dashed curve is below the solid curve demonstrates that the interaction energy between the “G” and “H” units is negative. We can understand this result by noting that, while the “G” units in the delimiting boundary (36.87°) are compressed, the “H” units in the other delimiting boundary (53.13°) are stretched. Combining the “G” and “H” units in an alternating fashion (i.e., at θ_{GH}) leads to a lower internal stress and hence a lower elastic energy and hence a negative interaction energy between the “G” and “H” units.

4.1.2. Elastic energy

In the misorientation range $\theta_X < \theta < \theta_{XY}$, the “Y” unit is the minority SU and can be thought of as a secondary GB dislocation on the “X” GB. The elastic energy due to an array of such dislocations is

$$\gamma^{el}(\theta) = \frac{\mu b_Y^2}{4\pi(1-\nu)D_Y} \ln\left(\frac{eD_Y}{2\pi r_Y}\right), \quad (4)$$

where μ is the shear modulus, ν the Poisson ratio, e the base of the natural logarithm, $D_Y = p/n_Y$ the spacing between the “Y” units, r_Y the dislocation core size, and b_Y the Burgers vector of the dislocations associated with the “Y” unit:

$$b_Y = 2p_Y \sin\left(\frac{\theta_Y - \theta_X}{2}\right). \quad (5)$$

Eq. (4) can also be applied in the $\theta_{XY} < \theta < \theta_Y$ range by replacing “X” with “Y”.

When the misorientation range ($\theta_Y - \theta_X$) is large, it helps to

modify the expression for the elastic energy as suggested by Li [41]:

$$\gamma^{el}(\theta) = \frac{\mu b_Y^2}{4\pi(1-\nu)D_Y} \left[\eta^* \coth \eta^* - \ln(2 \sinh \eta^*) - \frac{\eta_0^2}{2} \operatorname{csch}^2 \eta^* \right], \quad (6)$$

where $\eta_0 \equiv \pi r_Y/D_Y$ and η^* is the solution of $\eta^* \tanh \eta^* = \eta_0^2$. This expression takes into account the stress field of the cores of the GB dislocations and, thus, gives a more accurate prediction of the elastic interaction for dislocations when the cores get close together (as required for misorientations far from the delimiting boundaries) than Eq. (4).

The black solid curve in Fig. 5(a) shows an example of the effect of the elastic energy on the GB energy, where we have written the total GB energy as the sum of the core energy (Eq. (2); i.e., the solid blue curve in Fig. 5(a)) and the elastic energy (Eq. (6)) along the G-H path. Technically, when we apply Eq. (4), we choose r_X and r_Y to make γ^{el} continuous at θ_{XY} . However, when we apply Eq. (6), we choose r_X and r_Y based purely on geometry, that is as half of the sizes of the “X” and “Y” units.

In the treatment of the elastic energy above, we explicitly assumed isotropic elasticity. Clearly, many materials of interest exhibit significant elastic anisotropy. Extension of the present results to the anisotropic case may be obtained using standard methods of the anisotropic elastic theory of dislocations [42]. Unfortunately, the anisotropic results are not easily represented in closed form nor are they sufficiently physically transparent for an initial exposition as presented here. Interestingly, we note that the dominant contribution to the energy of high-angle GBs in metals is associated with the core structure (rather than elasticity) and that different forms of the elastic energy only affects the detailed shape of the GB energy vs. misorientation. In fact, most previous studies of GB energy vs. misorientation (based on other models) have assumed isotropic elasticity and found that this approximation works well for materials where the anisotropy is considerably larger than that in tungsten (e.g., see Refs. [37,38,40]).

4.1.3. Recursive construction of cusps

The elastic energy γ^{el} produces deep cusps in the GB energy γ at the misorientations of the delimiting boundaries (described by the “X” and “Y” units). The simulation data, however, show shallower cusps at other values of θ that are not reproduced. The fact that such shallow cusps are missing may be traced to the assumption that GB dislocations are evenly distributed. However, this is not necessarily true since, for example, it is not possible to have a ratio of $n_X : n_Y = 3 : 2$ ($|XXYXY|$) where the minority “Y” units are evenly spaced. We can include such an effect for this example by choosing the SUs in the delimiting boundaries as $|X|$ and $|XY|=“Z”$ (i.e., a MURS). Thus, $|XXYXY| = |XZZ|$, where now the “X” units are uniformly distributed amongst the “Z” units. Then, Eq. (4) or Eq. (6) can be applied within the misorientation range delimited by the GBs composed of “X” and “Z” units. This will lead to a new cusp in γ at the delimiting boundary described by only “Z” units. Of course, there are now cases where it is not possible to evenly distribute the “X” and “Z” units along the boundary (consider the case $n_X : n_Z = 3 : 2$). Hence, this same procedure can be applied again and again (recursively) until the GB energy is properly described (to our satisfaction).

In practice, we may implement the recursive construction as follows. Starting from the delimiting boundaries with “X” and “Y” units, we apply Eq. (2) and Eq. (6) to predict the GB energy γ for the intervening boundaries. However, the predicted γ values are considered correct only for the GBs whose structures correspond to an array of evenly distributed dislocations. Then, these GBs constitute a set of new delimiting boundaries through the

definition of MURS. Within each misorientation range enclosed by a pair of neighboring, already-defined delimiting boundaries, we use Eq. (2) and Eq. (4) to predict γ . Such procedure is performed recursively. We can find that, after each recursion step, we will obtain a set of cusps (corresponding to all the already-defined delimiting boundaries) and the depth of the additional cusps becomes smaller. The red solid curve in Fig. 5(a) shows the predicted γ along the G-H path after five recursion steps. The red dashed curve in Fig. 5(a) is the same as the red solid curve except that we also make use of another atomistic simulation to find the exact energy $\gamma(\theta_{GH})$. Comparison of this prediction with the atomistic simulation data (see Fig. 5(b)) shows that this recursive construction successfully captures all of the cusps seen in the simulation data.

In summary, based on the identity of the two original delimiting boundaries, we can predict the GB energy of the intervening boundaries by applying Eq. (2) and Eq. (6) and, then, recursively improving the prediction by application of Eq. (4). Through such a procedure, we can obtain a good prediction of the GB energy (as demonstrated by comparison with the atomistic simulation results), including the cusps and all possible GBs between these cusps.

4.2. Asymptotic strategy for energy prediction

Our ultimate aim is to predict the GB energy throughout the entire misorientation range. Yet, we would like to be able to take advantage of all of the data that is available and/or iteratively improve our prediction by performing a small number of additional (experimental or simulation) measurements.

4.2.1. Level of hierarchy

Our first step in predicting the GB energy vs. misorientation is to decide which boundaries are more “important” than others. The SUM suggests that delimiting boundaries are the most important boundaries in the sense that they play a key role in describing all of the intervening boundaries, as discussed above. For example, consider the case of the [100] STGBs. The first-order delimiting boundaries are those at $\theta = 0$ and 90° (characterized by the “A” and “B” units, respectively) since all intervening GBs for $0 < \theta < 90^\circ$ can be constructed from “A” and “B” units. The second-order GB is the one characterized by “[AB]” units ([AB] emphasizes that the AB structure can be re-defined as a SU, i.e., MURS); the GBs between θ_A and θ_{AB} can be described by “A” and “[AB]” units and those between θ_{AB} and θ_B by “[AB]” and “B” units. The third-order GBs are those characterized by “[A[AB]]” or “[AB]B” units; then, the rest GBs are composed of “A” and “[A[AB]]” units, “[A[AB]]” and “[AB]” units, “[AB]” and “[AB]B” units, or “[AB]B” and “B” units. Following this procedure, we can iteratively find higher and higher-order GBs. The lower-order GBs are more important than higher-order ones for predicting GB structure and energy.

Among a set of GBs of the same order, the most important GB is the one that, together with all of the lower-order GBs, divide the misorientation range into the most uniform set segments (in θ). As discussed above (and in Ref. [1]), the larger the misorientation range to which the energy formula is applied, the less accurate the energy prediction. Therefore, dividing the misorientation range as uniformly as possible should lead to the best prediction. For example, there are two third-order GBs, characterized by “[A[AB]]” and “[AB]B” units, respectively. If we consider the GB composed of “[A[AB]]” units as the additional delimiting boundary, then the largest misorientation range ($\Delta\theta_{max}$) delimited by the first-order, the second-order and this additional third-order GBs will be $\Delta\theta_{max} = 53.13^\circ$. However, if we consider the third-order GB to be composed of “[AB]B” units, $\Delta\theta_{max} = 36.87^\circ$. Therefore, the GB composed of “[AB]B” units is more important (for predicting $\gamma(\theta)$)

than that composed of “[A[AB]]” units.

In this way, we rank each GB (at different θ) according to the criteria: (1) lower-order delimiting boundary and (2) smaller misorientation range. With this ranking, we adopt a hierarchical procedure for predicting $\gamma(\theta)$ by prioritizing the acquisition of GB energy data from lower-rank GBs to higher-rank GBs. We define the level of hierarchy κ as the largest-rank GB used in our prediction minus one. For $\kappa = 0$, the only information we employ is for the $\theta = 0$ and 90° (first rank) GBs. For any level κ , the required input is for all the $(\kappa' + 1)^{th}$ -rank GBs ($0 \leq \kappa' \leq \kappa$).

The GBs associated with a few of the smallest κ values are listed in Table 2 for both [100] and [111] STGBs in BCC materials. Increasing κ tends to decrease the largest misorientation range $\Delta\theta_{max}$ divided by the delimiting boundaries and tends to increase the Σ value, the size of GB period p , and the number of metastable structures M .

4.2.2. Asymptotic approach

Based on the GB level of hierarchy idea, we now outline an asymptotic approach to estimating the GB energy over the entire misorientation range.

- (1) Start from two $\kappa = 0$ GBs (e.g., perfect crystal at $\theta = 0$ and 90° for [100] STGBs); these are the original pair of delimiting boundaries. We may find multiple metastable structures for each of these in atomistic simulations. Choose a pair of SUs (one from each of the two delimiting boundaries) and estimate the energy of the intervening boundaries corresponding to combinations of this pair of SUs (using the energy formulae in Section 4.1). Do this for all possible pairs of SUs from these delimiting boundaries and obtain $\gamma(\theta)$ curves associated with all of these structure-evolution paths.
- (2) Let $\kappa' = \kappa + 1$ and consider the κ' GB; the κ' GB is an additional delimiting boundary with a misorientation that lies between the two lower-level delimiting boundaries. We denote the sets of metastable SUs of these two lower-level delimiting boundaries as $\{X_m\}$ and $\{Y_n\}$ (m and n identify the different stable/metastable SUs), respectively. From the

Table 2

The GBs corresponding to several of the lowest levels of hierarchy (κ). For each GB, we list κ , the order for this GB as a delimiting boundary, the misorientation (θ), the Σ value, the size of the GB period along the direction \mathbf{p} (p), and the maximum misorientation range delimited by the GBs with level $\leq \kappa$ ($\Delta\theta_{max}$), the GB structure in the form of SUs (“[•]” indicates MURS), and the number of metastable structures (M).

κ	Order	θ ($^\circ$)	Σ	p (a_0)	$\Delta\theta_{max}$ ($^\circ$)	Form of SU	M
[100] STGBs in BCC							
0	1	0	1	1	90	A	1
0	1	90	1	0.7071	90	B	1
1	2	36.87	5	1.5811	53.13	[AB]	2
2	3	53.13	5	2.2361	36.87	[[AB]B]	3
3	3	22.62	13	2.5495	28.07	[A[AB]]	1
3	4	61.93	17	2.9155	28.07	[[[AB]B]B]	5
4	5	67.38	13	3.6056	22.62	[[[[AB]B]B]B]	7
5	4	16.26	25	3.5355	18.92	[A[A[AB]]]	1
5	6	71.08	37	4.3012	18.92	[[[[[AB]B]B]B]B]	7
6	7	73.74	25	5	16.26	[[[[[AB]B]B]B]B]B]	10
[111] STGBs in BCC							
0	1	0	1	0.8165	60	A	1
0	1	60	3	1.4142	60	B	1
1	2	38.21	7	2.1602	38.21	[AB]	4
2	3	27.80	13	2.9439	27.80	[A[AB]]	5
3	4	21.79	21	3.7417	21.79	[A[A[AB]]]	3
4	5	17.90	31	4.5461	17.90	[A[A[A[AB]]]]	5
4	3	46.83	19	3.5590	17.90	[[AB]B]	5
5	6	15.18	43	5.3541	15.18	[A[A[A[A[AB]]]]]	7
6	7	13.17	57	6.1644	13.17	[A[A[A[A[A[AB]]]]]]	10

previous steps, we know the structures and energies corresponding to $\{X_m\}$ and $\{Y_n\}$, and have predicted the structures of the intervening GBs (including the κ' GB) as combinations of all possible “ X_m ” and “ Y_n ” units and their energies (denoted by $\gamma_{mn}(\theta)$). Now, by atomistic simulations, we may find the exact metastable structures and energies of the κ' GB. We correct the $\gamma(\theta)$ prediction (from the previous steps) using these simulation results by examining the following situations:

- (i) If no metastable structure of the κ' GB composed of the “ X_m ” and “ Y_n ” units is found, delete the energy curve $\gamma_{mn}(\theta)$ in the $\theta_X < \theta < \theta_Y$ range (see Fig. 6(a)).
- (ii) If there is one metastable structure of the κ' GB composed of a new SU (denoted by “Z”), which cannot be represented by combination of “ X_m ” and “ Y_n ” units, then add a new GB energy curve in the $\theta_X < \theta < \theta_Z$ range estimated by taking “ X_m ” and “Z” units as the delimiting boundaries (using the energy formulae in Section 4.1), and, similarly, add a new GB energy curve in the $\theta_Z < \theta < \theta_Y$ range estimated by taking “Z” and “ Y_n ” units as the delimiting boundaries (see Fig. 6(b)).
- (iii) If there is a metastable structure of the κ' GB corresponding to a combination of “ X_m ” and “ Y_n ” units, modify the energy curve $\gamma_{mn}(\theta)$ (predicted in the previous steps) according to the exact energy from the atomistic simulation (see Fig. 6(c)).
- (3) Let $\kappa := \kappa'$ and repeat Step (2) until further iterations no longer change the GB energy to within whatever accuracy we choose to specify. Since each new iteration requires another atomistic simulation, this stop condition should represent a balance between accuracy and computational efficiency.

Following the procedure above, the predicted minimum GB energy should asymptotically approach the exact result for the entire misorientation range (where “exact” implies that obtained from an infinite number of atomistic simulations). This strategy balances the trade-off between the amount of information used to make the prediction and the accuracy of the prediction. This balance could be struck in two ways: first, giving the best possible

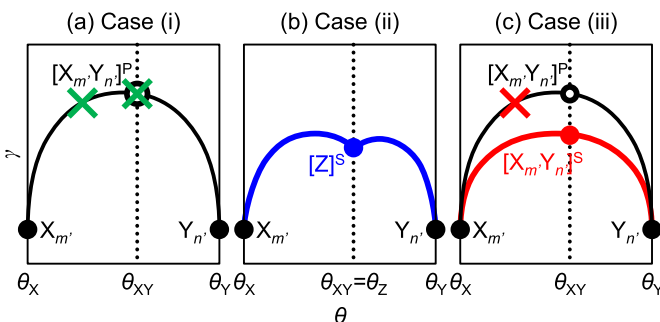


Fig. 6. Modification of the predicted GB energy (see Section 4.1) for $\theta_X < \theta < \theta_Y$ based on the GB structure/energy at $\theta = \theta_{XY}$ as determined from an atomistic simulation for the three cases in Step (2) in Section 4.2.2. The black solid curve shows the predicted GB energy based on the delimiting boundaries composed of only “ X_m ” and only “ Y_n ” units. The open circles label the predicted energy for the intervening boundary described by the combination of the “ X_m ” and “ Y_n ” units, denoted by “[$X_m Y_n$]^P” (“P” indicates prediction). The solid circles correspond to the GB energies obtained from simulation. (a) If the structure [$X_m Y_n$]^P is not found in the simulation, the black solid curve does not exist. (b) If a new structure based on a SU [Z]^S (“S” indicates simulation result) is found in the simulation, add the blue solid curve. (c) If the structure [$X_m Y_n$]^S is found in the simulation, replace the (predicted) black solid curve with the red solid curve that goes through the energy of [$X_m Y_n$]^S. (For interpretation of the references to colour in this figure legend, the reader is referred to the web version of this article.)

estimate of the GB energy based on a limit set of data and second, iteratively improving the accuracy of the prediction by including ever more data into the prediction.

4.2.3. Energy prediction examples

Fig. 7(a) shows an example of the application of this asymptotic approach for [100] STGBs in BCC tungsten. There are two $\kappa = 0$ GBs, characterized by “A” and “B” units, corresponding to the (001) and (011) planes in a BCC crystal. Assuming all GBs had structures composed solely of “A” and “B” units, we can predict the energy for the A-B path (using the procedure in Section 4.1), as shown in Fig. 7(a1); this is our estimate of the GB energy based on no data at all.

We can improve our original estimate by performing a simulation on the $\kappa = 1$ GB with $\theta = 36.89^\circ$ (see Table 2); the simulations show that there are two metastable structures, $|C \cdot C|$ (or, equivalently, $|E \odot E \odot E \odot E|$) and $|AB \cdot AB|$. We can modify the energy of the A-B path based on the energy of the “AB” unit and also predict two new energy paths based on the two new metastable structures, i.e., the A-C-B and A-E-B paths, as shown in Fig. 7(a2).

For the next level ($\kappa = 2$), we perform atomistic simulations at $\theta = 53.13^\circ$ and find that there are three metastable structures: $|C \cdot B|$ (or, equivalently, $|E \odot EB|$), $|D|$ and $|AB \cdot B|$. Based on these three structures we modify the A-B, A-C-B and A-E-B paths. However, because we find three metastable states at $\theta = 53.13^\circ$, we also determine the energies of the new paths: the C-D-B, G-D-B (“G”≡“AB”), C-I (“I”≡“ABA”) and G-H (“H”≡“CB”) paths (cf. Figs. 3 and 4 for structures), as shown in Fig. 7(a3).

If we perform simulation for the $\theta = 22.62^\circ$ and 61.93° ($\kappa = 3$) GBs, we can further improve our energy prediction, as shown in Fig. 7(a4). This procedure can be performed at higher and higher κ values, adding atomistic simulation data at one or two additional values of θ for each. Fig. 7(a5) and (a6) show the predictions with inclusion of the data for the $\kappa = 4$ and 5 GBs, respectively. We note that the minimum GB energy curves for $\kappa = 3, 4$ and 5 are nearly identical. This demonstrates that it is possible to truncate the iterative refinement at very small levels of κ , i.e., with data based on simulations at very few misorientations (for $\kappa = 3$, simulations at only four misorientations are required). The thick light blue curve in Fig. 7 corresponds to the atomistic simulation data obtained for a very large number of misorientations. By using the data from four simulations ($\kappa = 3$) in prediction, we can accurately reproduce the entire, large set of simulation data; i.e., reducing the requisite number of misorientations simulated from 110 to only four without sacrificing accuracy. We note that, since the four simulations required are for relatively high symmetry boundaries (compared with many of those in the data set consisting of 110 simulations), the computational savings is more than two orders of magnitude.

In order to examine the generality of the approach described above, we examine the GB energy vs. misorientation for another set of GBs ([111] STGBs) in the same material (tungsten). The results are shown in Fig. 7(b). Again we see that (i) the predicted minimum GB energy curves become nearly independent of κ for $\kappa \geq 3$ and (ii) the predicted GB energy vs. misorientation curve is an accurate reproduction of the results from the entire set of simulations for all for 52 orientations (in this case, the predictions were made based on simulations at only three misorientations).

We re-plot the minimum GB energy vs. misorientation predictions together with the results from a large number of simulations for both the [100] and [111] STGBs in Fig. 8(a) and (b). While this does again show the excellent correspondence between prediction and simulation, we can also see that the GBs along the minimum-energy path come from a wide range of different structure-evolution paths (indicated by the solid curves with different color in Fig. 8(a) and (b)). For example, the A-C path

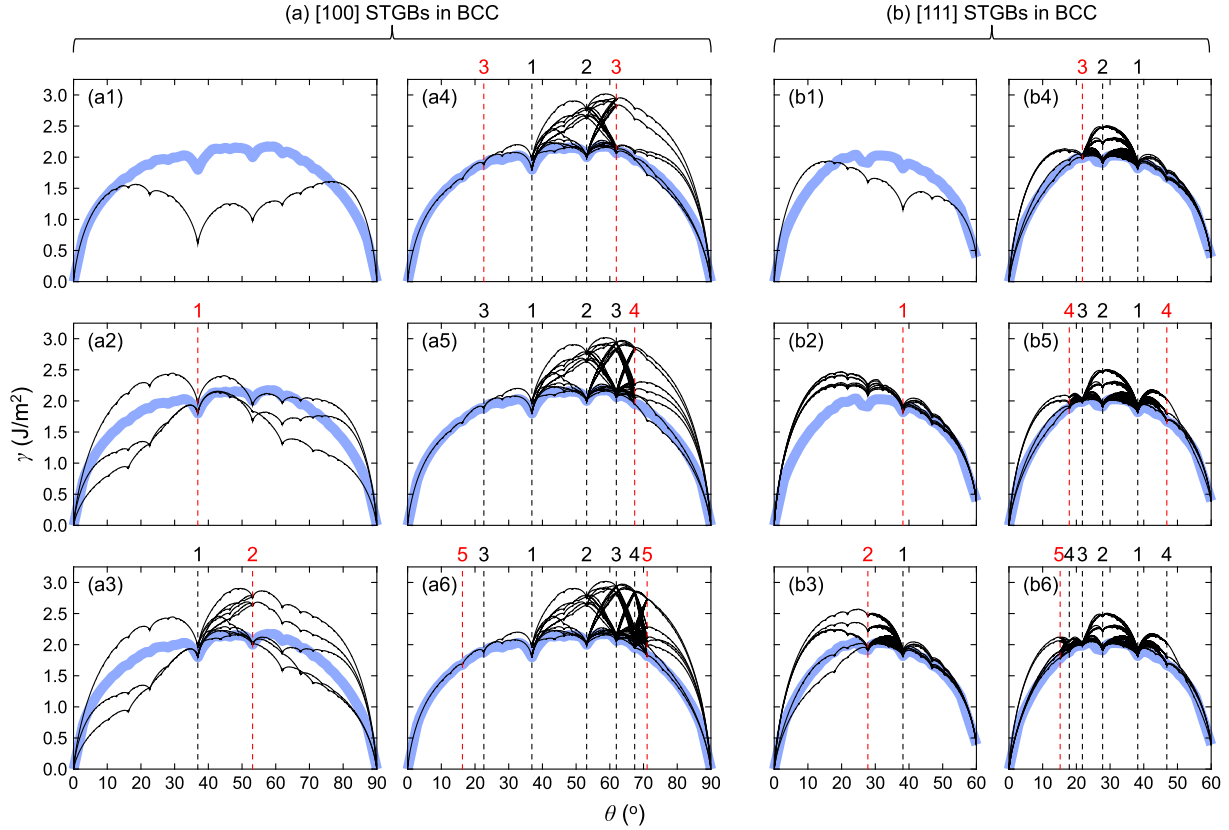


Fig. 7. Implementation of the asymptotic strategy for the prediction of GB energy vs. misorientation exemplified by two cases: (a) [100] and (b) [111] STGBs in BCC tungsten. In each plot, the dashed lines label the GBs whose structures and energies were determined from the simulations and used in the prediction, and the light blue curve denote the minimum GB energy obtained by the simulations. The integer above each dashed line indicates the level of hierarchy of the corresponding GB. The red dashed lines denote the GBs with the highest level used in the prediction. From (a1) to (a6), or from (b1) to (b6), the prediction is improved step by step by considering the GBs with higher and higher κ values. (For interpretation of the references to colour in this figure legend, the reader is referred to the web version of this article.)

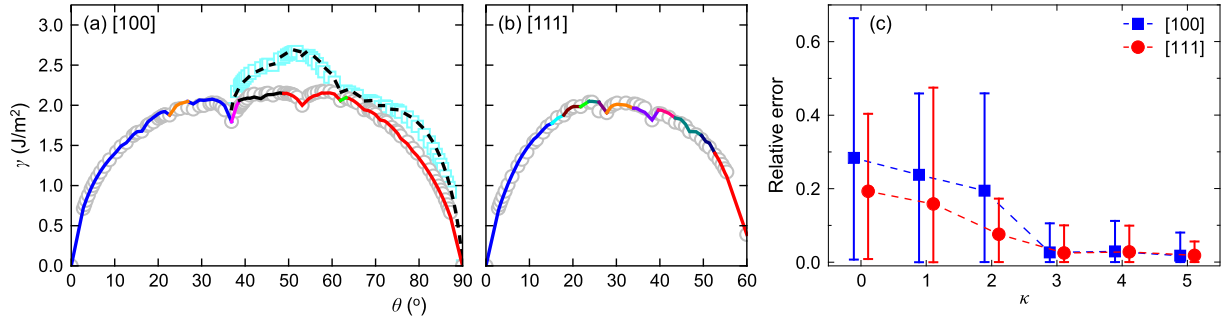


Fig. 8. Comparison between the predicted GB energy and the simulation data for (a) [100] and (b) [111] STGBs in BCC tungsten. The solid curves represent the predicted minimum GB energy, and the gray open circles are the simulation data for the minimum GB energy. The segments with different colors on the solid curves indicate different structure-evolution paths (i.e. combination of different SUs). In (a), the dashed curve represents the predicted GB energy for the G-D-B path (see Fig. 3(c)) while the light blue squares are the simulation data. (c) The relative error of the prediction (defined in the text) vs. the level of hierarchy used in the prediction (κ). The upper and lower bounds of the error bar denote the largest and the smallest error throughout the entire misorientation range, respectively. (For interpretation of the references to colour in this figure legend, the reader is referred to the web version of this article.)

($0 \leq \theta \leq 36.87^\circ$) in the GB energy, shown as the solid blue curve in Fig. 8(a), is interrupted by another structure-evolution path (the solid orange curve). This confirms our assertion that, while the main idea of describing the GB energy vs. misorientation based on the SUM is valid, it must be applied based on many metastable SUs in order to obtain an accurate reproduction of the true minimum GB energy vs. misorientation. We also note that the results of same quality can be obtained not simply for the minimum-energy curve, but also for the higher-energy curves (corresponding to metastable

structure-evolution paths); see the results in Fig. 8(a) for the G-D-B path ($36.87^\circ \leq \theta \leq 90^\circ$) and Fig. 5(b) for the G-H path ($36.87^\circ \leq \theta \leq 53.13^\circ$) for the [100] STGBs.

In order to better understand how the minimum GB energy curve converges with increasing κ , we examine the error in our predictions, where the relative error is defined as $|\gamma_{\min}^S - \gamma_{\min}^P|/\gamma_{\min}^S$ (γ_{\min}^S and γ_{\min}^P are the minimum GB energies obtained by simulation and prediction, respectively). The relative error varies with θ such that for each κ there is a distribution of

relative errors. In Fig. 8(c), we plot the mean value of this distribution (the relative error averaged over all θ) as data points as well as the maximum and minimum errors of this distribution (shown as the error bars). Again, we see that the predictions for both the [100] and [111] STGBs converge by $\kappa = 3$. More interestingly, the mean relative error at this κ is smaller than 2% and the maximum relative error (considering all values of θ) is smaller than 11%. It is remarkable that this level of accuracy was achieved based on input from simulations performed at only three ([111] STGBs) or four ([100] STGBs) misorientations.

4.3. The number of metastable structures

In addition to the GB structure and energy vs. misorientation, we can also predict the number of metastable symmetry-unrelated GB structures based upon the metastable structural unit model (MSUM). Recall that the structure of any CSL GB can be represented in the form of $|XY|$, where “X” and “Y” represent different SUs. The number of metastable structures of the $|XY|$ GB, M_{XY} , can be deduced from the numbers of metastable structures of the $|X|$ and $|Y|$ GBs (i.e., M_X and M_Y). According to the rule of combination, $M_{XY} = M_X M_Y$; this is a recursive formula. M_{XY} determined in this manner actually represents the maximum possible number of metastable structure, but as we have seen above, some of these structures are unstable. By performing atomistic simulations we may determine how many of these M_X structures are stable and thereby “correct” our prediction. Like in our calculations of the GB energy, we can iteratively improve our prediction of the number of metastable GBs at each value of θ , $M(\theta)$, by including atomistic simulation data as dictated by the level of hierarchy, κ .

We tabulate the number of metastable structures for each misorientation in terms of the dimensionless uncertainty function (related to configurational entropy [24]) \tilde{s}_c , which is defined as

$$\tilde{s}_c(\theta) = \frac{a_0}{p(\theta)} \ln M(\theta), \quad (7)$$

where a_0 is the lattice constant. Fig. 9(a1) and (b1) show \tilde{s}_c vs. θ for the [100] and [111] STGBs in tungsten. In these figures, the predictions for $\kappa = 10$ and 40 are shown as the red dashed lines and the data based on a large set of simulations are shown as the yellow shaded region and the gray lines. Overall, these predictions successfully capture the major trends and magnitude of $\tilde{s}_c(\theta)$. Nonetheless, this prediction does generally lead to slightly higher values than is found from the simulations.

The overestimation of $\tilde{s}_c(\theta)$ may be attributed to the fact that we predict the total number of possible combinations of the metastable structures via the SUs from the delimiting boundaries and that some of these combinations are unstable. For example, we have shown that the structures belonging to combinations of “A” and “B” units are unstable for most misorientations (only a few such combinations are stable, as indicated by the dark green crosses in Fig. 2(a)). We can account for such unstable combinations in an empirical manner by simply assuming that a fraction ϵ of the predicted combinations are unstable. To predict the number of metastable states M for the i^{th} order GB (see Section 4.2.1 and Table 2), we need to consider the probability that each SU is stable ($1 - \epsilon$) for each of the lower orders; hence we adjust the predicted M by a factor of $(1 - \epsilon)^i$. More explicitly, the number of metastable structures of an i^{th} -order $|XY|$ GB is

$$M_{XY} = M_X M_Y (1 - \epsilon)^i. \quad (8)$$

Even if ϵ is much smaller than one, the correction factor can be significantly smaller than one when i is very large (i.e., for the high-

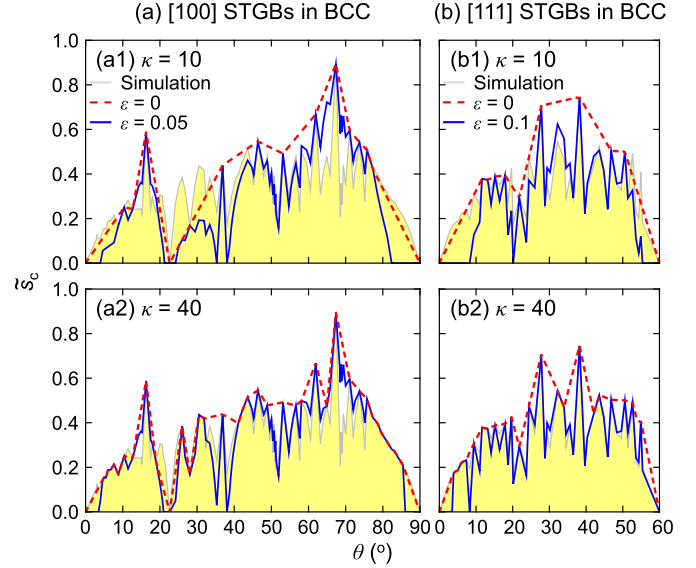


Fig. 9. The values of the uncertainty function \tilde{s}_c defined in Eq. (7) corresponding to all the misorientations for (a) [100] and (b) [111] STGBs in BCC tungsten. The yellow shaded regions and the solid gray lines represent the simulation data, the red dashed lines represent the prediction results without correction ($\epsilon = 0$), and the blue solid lines represent the prediction results with correction ($\epsilon = 0.05$ and 0.1 for [100] and [111] STGBs, respectively). The prediction was performed by inputting the information of the GBs up to the level $\kappa = 10$ for (a1) and (b1) and up to $\kappa = 40$ for (a2) and (b2). (For interpretation of the references to colour in this figure legend, the reader is referred to the web version of this article.)

order GBs). In practice, the ϵ value can be determined by fitting to the simulation data for the GBs for the several lowest κ values. The results are shown as the blue solid lines in Fig. 9, where $\epsilon = 0.05$ and 0.1 for [100] and [111] STGBs, respectively. Inclusion of this empirical correction yields a much better prediction for $\tilde{s}_c(\theta)$ as compared with the simulation results, including its serrations. This demonstrates that most of the serrations observed in $\tilde{s}_c(\theta)$ are attributable to unstable GB structures.

As discussed in Ref. [24], the uncertainty function \tilde{s}_c is related to the GB configurational entropy in far-from-equilibrium situations. It can be used to understand such disparate kinetic process as the absorption of point defects by GBs during irradiation damage and high-temperature viscous GB sliding. This suggests that GB metastability in the SUM (i.e., the MSUM) provides a much fuller understanding of GB properties, including nonequilibrium GB dynamical properties.

5. Influence of non-conservative sampling

As discussed above, we found different metastable GB structures in the atomistic simulations by exploring the space of relative displacement of one crystal with respect to the other where the displacement vectors lie in the GB plane. However, it is now widely recognized [22–24] that different GB structures may also be obtained by adding or removing atoms from the GB itself (so-called non-conservative sampling). Adding different number of atoms to the GB may result in different metastable structures; we define the atomic fraction in the GB plane ϕ as another microscopic degree of freedom of the GB in a bicrystal, where $\phi \equiv 1 - (\text{number of removed atoms}) / (\text{number of atoms per layer parallel to the GB})$. In this section, we demonstrate that the metastable structures explored by non-conservative sampling still follow the MSUM and constitute new structure-evolution path(s) along the energy-vs.-misorientation curve.

Consider the case of the $\Sigma 5$ (013) GB in tungsten. By varying ϕ , we found a new stable structure $|J \cdot J|$ corresponding to $\phi = 0.2$ (see Fig. 10); this structure differs from both the $|C \cdot C|$ and $|AB \cdot AB|$ structures we found previously based on conservative sampling. The period of the “J” unit is five times larger than that of the “C” or “AB” unit along the $\hat{\mathbf{o}}$ -axis (Fig. 10(b)). The atomic structure of a “J” unit along the $\hat{\mathbf{o}}$ -axis features a wavy deviation of the atomic coordinates in the $\hat{\mathbf{n}}$ -direction from the $(0\bar{3}1)$ plane (colored red in Fig. 10). The neighboring “J” unit has the same wavy feature but has a half-period phase shift along the $\hat{\mathbf{o}}$ -axis (colored blue in Fig. 10). If we take this GB and the GB with $\theta = 90^\circ$ (characterized by “B” units) as the two delimiting boundaries, then the intervening boundaries can be regarded as the combination of “J” and “B” units. Although we did not look at many intervening boundaries, from the results of the GBs with $\theta = 43.60^\circ$, 46.40° , 53.13° and 61.93° , we indeed found their structures composed of “J” and “B” units, implying a structure-evolution path, i.e., J-B path, from $\theta = 36.87^\circ$ to 90° (see Fig. 10(a)). It is possible that the existence of a “J” unit might be an artifice of the particular empirical interatomic potential (we did not examine this possibility here). However, by this example, we demonstrate the generality of SUM procedure with respect to GB metastability and demonstrate that it applies with equal validity to metastable states formed by non-conservative and conservative sampling.

6. Discussion and conclusions

We have extended the classical description of grain-boundary structure in terms of the structural unit model (SUM) to account for the fact that multiple metastable GB structures exist for most grain boundaries. Based on atomistic simulation and analysis of GB structure and energy, we conclude:

- (1) for each misorientation, there are several metastable structures. Each of these structure can be understood in terms of the SUM based on the structural units of appropriately

chosen delimiting boundaries. This leads to several distinct structure-evolutions paths (i.e., structure vs. misorientation).

- (2) The minimum GB energy vs. misorientation $\gamma(\theta)$ (i.e., low-temperature equilibrium GB energy) is determined by many, often intersecting $\gamma(\theta)$ curves corresponding to multiple structure-evolution paths.
- (3) Inclusion of the multiple structure-evolution paths leads to a new method to accurately predict the GB structure and energy over the entire misorientation range based on very few atomistic simulations. This approach can be applied in a manner that permits a trade-off between prediction accuracy and computational cost.

We have demonstrated (via extensive atomistic simulations) the accuracy of our predictions of $\gamma(\theta)$ for a series of [100] symmetric tilt boundaries ($0 \leq \theta \leq 90^\circ$) in tungsten based on only four (short-period) GB simulations and for a series of [111] symmetric tilt boundaries ($0 \leq \theta \leq 60^\circ$) based on only three GB simulations.

In this paper, we have focused our discussion of the metastable structural unit model (MSUM) to the case of symmetric tilt boundaries rather than examining all five macroscopic parameters describing GB bicrystallography. We emphasize, however, that the same approach is applicable to all GBs. We note that the early applications of the SUM have also considered the structure and the energy of asymmetric tilt and twist boundaries; the same approaches may be followed in the application of the MSUM to such GBs. The extension from symmetric to asymmetric tilt boundaries is straightforward. For faceted asymmetric tilt boundaries, we only need to know the energy associated with the facets which are symmetric tilt boundaries [43]. Non-faceted asymmetric tilt boundaries can be viewed as a combination of the structural units in the same manner as for symmetric tilt boundaries [15]. Thus, if we know the possible stable and/or metastable structural units, we can predict the GB energy of non-faceted asymmetric boundaries following exactly the same approach discussed above. While the same approach may be applied to twist boundaries, this extension

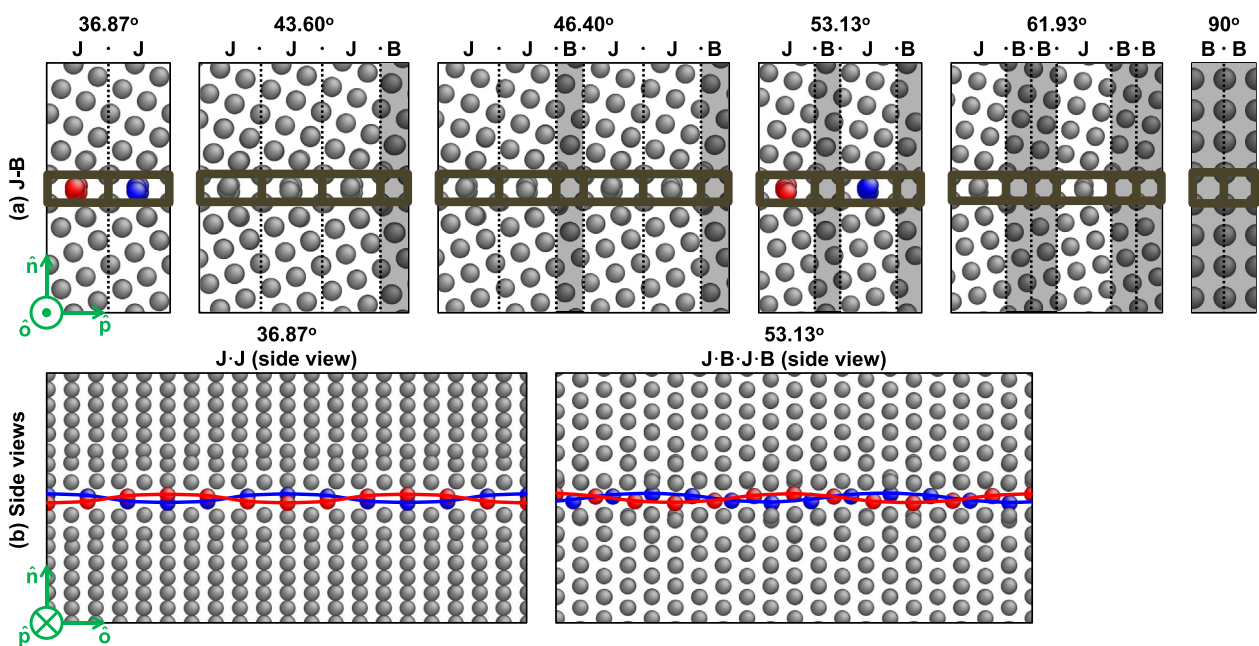


Fig. 10. (a) GB structures represented by “J” and “B” units. These structures are obtained by varying the atomic fraction in the GB plane. (b) The side views of the $|J \cdot J|$ and $|J \cdot B \cdot J \cdot B|$ structures corresponding to the front views shown in (a) for $\theta = 36.87^\circ$ and 53.13° . An array of atoms centered in a “J” unit are colored red and another array of atoms in the neighboring “J” unit are colored blue. (b) shows two arrays of the colored atoms that exhibit a wavy arrangement along the $\hat{\mathbf{o}}$ -axis. (For interpretation of the references to colour in this figure legend, the reader is referred to the web version of this article.)

is less straightforward, despite the fact that twist boundaries may also be described as combinations of structural units [44]. Because twist boundaries may be thought of as two-dimensional arrangements of structural units, the expressions for the elastic and core energies must include integrals (or summations) over both dimensions (e.g., Ref. [45]).

Acknowledgment

D.J.S. acknowledges support of the National Science Foundation Division of Materials Research through Award No. DMR-1507013.

References

- [1] A.P. Sutton, R.W. Balluffi, *Interfaces in Crystalline Materials*, Oxford University Press, 1995.
- [2] W. Rosenhain, J.C.W. Humfrey, The tenacity, deformation, and fracture of soft steel at high temperatures, *Iron Steel Inst* 87 (1913) 219.
- [3] S.R. Phillpot, D. Wolf, H. Gleiter, A structural model for grain boundaries in nanocrystalline materials, *Scr. Metall. Mater* 33 (1995) 1245–1251.
- [4] T.-S. Ké, Experimental evidence of the viscous behavior of grain boundaries in metals, *Phys. Rev.* 71 (1947) 533–546.
- [5] T.E. Hsieh, R.W. Balluffi, Experimental study of grain boundary melting in aluminum, *Acta Metall.* 37 (1989) 1637–1644.
- [6] G. Duscher, M.F. Chisholm, U. Alber, M. Rühle, Bismuth-induced embrittlement of copper grain boundaries, *Nat. Mater* 3 (2004) 621–626.
- [7] G.I. Taylor, The mechanism of plastic deformation of crystals. part ii. comparison with observations, *Proc. R. Soc. Lond. A* 145 (1934) 388–404.
- [8] J.M. Burgers, Some Considerations on the Fields of Stress Connected with Dislocations in a Regular Crystal Lattice. I, vol. 42, Koninklijke Nederlandse Akademie van Wetenschappen, 1939.
- [9] W.T. Read, W. Shockley, Dislocation models of crystal grain boundaries, *Phys. Rev.* 78 (1950) 275.
- [10] B.A. Bilby, Types of dislocation source, in: Report of Bristol Conference on Defects in Crystalline Solids, The Physical Soc. Bristol 1954, London, 1955, pp. 124–133.
- [11] F.C. Frank, The resultant content of dislocations in an arbitrary intercrystalline boundary, in: Symposium on the Plastic Deformation of Crystalline Solids, Pittsburgh, Pennsylvania, 1950, p. 150.
- [12] J.P. Hirth, R.C. Pond, R.G. Hoagland, X.-Y. Liu, J. Wang, Interface defects, reference spaces and the frank-bilby equation, *Prog. Mater. Sci.* 58 (2013) 749–823.
- [13] G.H. Bishop, B. Chalmers, A coincidence-ledge-dislocation description of grain boundaries, *Scr. Metall.* 2 (1968) 133–139.
- [14] A.P. Sutton, V. Vitek, On the structure of tilt grain boundaries in cubic metals i. symmetrical tilt boundaries, *Phil. Trans. R. Soc. Lond. A* 309 (1983) 1–36.
- [15] A.P. Sutton, V. Vitek, On the structure of tilt grain boundaries in cubic metals ii. asymmetrical tilt boundaries, *Phil. Trans. R. Soc. Lond. A* 309 (1983) 37–54.
- [16] A.P. Sutton, V. Vitek, On the structure of tilt grain boundaries in cubic metals iii. generalizations of the structural study and implications for the properties of grain boundaries, *Phil. Trans. R. Soc. Lond. A* 309 (1983) 55–68.
- [17] J.D. Ritter, D.N. Seidman, {110} symmetric tilt grain-boundary structures in fcc metals with low stacking-fault energies, *Phys. Rev. B* 54 (1996) 6999.
- [18] D.N. Pawaskar, R. Miller, R. Phillips, Structure and energetics of long-period tilt grain boundaries using an effective hamiltonian, *Phys. Rev. B* 63 (2001) 214105.
- [19] V. Vitek, Y. Minonishi, G.J. Wang, Multiplicity of grain boundary structures: vacancies in boundaries and transformations of the boundary structure, *J. Phys. Paris.* 46 (1985) C4 171.
- [20] Y. Oh, V. Vitek, Structural multiplicity of $\sigma = 5$ (001) twist boundaries and interpretation of x-ray diffraction from these boundaries, *Acta Metall.* 34 (1986) 1941–1953.
- [21] W. Krakow, Structural multiplicity observed at a sigma=5/[001] 53.1 tilt boundary in gold, *Philos. Mag. A* 63 (1991) 233–240.
- [22] S. von Alftan, P.D. Haynes, K. Kaski, A.P. Sutton, Are the structures of twist grain boundaries in silicon ordered at 0 k? *Phys. Rev. Lett.* 96 (2006) 055505.
- [23] T. Frolov, D.L. Olmsted, M. Asta, Y. Mishin, Structural phase transformations in metallic grain boundaries, *Nat. Comm.* 4 (2013) 1899.
- [24] J. Han, V. Vitek, D.J. Srolovitz, Grain-boundary metastability and its statistical properties, *Acta Mater.* 104 (2016) 259–273.
- [25] D. Wolf, High-temperature structure and properties of grain boundaries: long-range vs. short-range structural effects, *Curr. Opin. Solid State Mater. Sci.* 5 (2001) 435–443.
- [26] H. Zhang, D.J. Srolovitz, J.F. Douglas, J.A. Warren, Grain boundaries exhibit the dynamics of glass-forming liquids, *Proc. Natl. Acad. Sci. U.S.A.* 106 (2009) 7735–7740.
- [27] K.H. Nagamanasa, S. Gokhale, R. Ganapathy, A.K. Sood, Confined glassy dynamics at grain boundaries in colloidal crystals, *Proc. Natl. Acad. Sci. U.S.A.* 108 (2011) 11323–11326.
- [28] J.J. Bean, K.P. McKenna, Origin of differences in the excess volume of copper and nickel grain boundaries, *Acta Mater.* 110 (2016) 246–257.
- [29] X. Zhou, D. Marchand, D.L. McDowell, T. Zhu, J. Song, Chemomechanical origin of hydrogen trapping at grain boundaries in fcc metals, *Phys. Rev. Lett.* 116 (2016) 075502.
- [30] R. Dingreville, S. Berbenni, On the interaction of solutes with grain boundaries, *Acta Mater.* 104 (2016) 237–249.
- [31] R. Li, H.B. Chew, Grain boundary traction signatures: quantitative predictors of dislocation emission, *Phys. Rev. Lett.* 117 (2016) 085502.
- [32] G.J. Ackland, R. Thetford, An improved n-body semi-empirical model for body-centred cubic transition metals, *Philos. Mag. A* 56 (1987) 15–30.
- [33] P.D. Bristowe, R.W. Balluffi, Structural unit/grain boundary dislocation model for twist boundaries in cubic crystals, *J. Phys. Colloq.* 46 (1985) C4–C155.
- [34] A.P. Sutton, R.W. Balluffi, V. Vitek, On intrinsic secondary grain boundary dislocation arrays in high angle symmetrical tilt grain boundaries, *Scr. Metall.* 15 (1981) 989–994.
- [35] D. Chen, S. Cai, Z. Suo, R.C. Hayward, Surface energy as a barrier to creasing of elastomer films: an elastic analogy to classical nucleation, *Phys. Rev. Lett.* 109 (2012) 038001.
- [36] D.A. Porter, K.E. Easterling, M.Y. Sherif, *Phase Transformations in Metals and Alloys*, CRC Press, 2009.
- [37] P.R.M. van Beers, V.G. Kouznetsova, M.G.D. Geers, M.A. Tschoop, D.L. McDowell, A multiscale model of grain boundary structure and energy: from atomistics to a continuum description, *Acta Mater.* 82 (2015) 513–529.
- [38] V.V. Bulatov, B.W. Reed, M. Kumar, Grain boundary energy function for fcc metals, *Acta Mater.* 65 (2014) 161–175.
- [39] B. Runnels, I.J. Beyerlein, S. Conti, M. Ortiz, An analytical model of interfacial energy based on a lattice-matching interatomic energy, *J. Mech. Phys. Solids* 89 (2016) 174–193.
- [40] G.-J. Wang, V. Vitek, Relationships between grain boundary structure and energy, *Acta Metall.* 34 (1986) 951–960.
- [41] J.C.M. Li, High-angle tilt boundary – a dislocation core model, *J. Appl. Phys.* 32 (1961) 525–541.
- [42] A.N. Stroh, Dislocations and cracks in anisotropic elasticity, *Philos. Mag.* 3 (1958) 625–646.
- [43] A. Brokman, P.D. Bristowe, R.W. Balluffi, Atomistic faceting of asymmetric tilt boundaries, *Scr. Metall.* 15 (1981) 201–206.
- [44] D. Schwartz, V. Vitek, A.P. Sutton, Atomic structure of (001) twist boundaries in fcc metals structural unit model, *Philos. Mag. A* 51 (1985) 499–520.
- [45] S. Dai, Y. Xiang, D.J. Srolovitz, Structure and energy of (111) low-angle twist boundaries in al, cu and ni, *Acta mater.* 61 (2013) 1327–1337.